

## RESEARCH ARTICLE

# A Broadband Multimode Antenna With Enhanced Gain and High Efficiency by Employing Metasurface for WLAN and Car-to-Car Application

YAQIANG ZHENG<sup>1,2</sup>, MIN GAO<sup>1,3</sup>, AND XIAOHU ZHAO<sup>1,4</sup><sup>1</sup>School of Information and Control Engineering, China University of Mining and Technology, Xuzhou 221000, China<sup>2</sup>School of Intelligent Manufacturing, Huainan Union University, Huainan 232000, China<sup>3</sup>School of Mechanical and Electrical Engineering, Hefei Technology College, Hefei 230601, China<sup>4</sup>National Joint Engineering Laboratory of Internet Applied Technology of Mines, Xuzhou 221000, China

Corresponding author: Xiaohu Zhao (zhaoxiaohu@cumt.edu.cn)

This work was supported in part by the Fundamental Research Funds for the Central Universities under Grant 2020ZDPY0223, and in part by the Natural Science Research Funds Project of Hefei Technology College under Grant 2021KJA01.

**ABSTRACT** A multimode resonance patch antenna with the attractive radiation gain and efficiency is investigated in this paper. A driven patch with both sides shorted similar to the cavity model is presented to generate  $TM_{03}$  and  $TM_{11}$  modes.  $TM_{21}$  mode is also excited by inserting five shorting parasitic patches on both sides of the radiation aperture to extend the impedance bandwidth and no additional feeding structure is required. Meanwhile, a novel metasurface with the positive gradient of the reflection phase is placed directly above the proposed multimode antenna. Then the characteristics of high gain and better front-to-back ratio (FBR) are acquired. The measured results show that the characteristics of 20.7% impedance bandwidth from 5.08 GHz to 6.25 GHz, stable gain of up to 12.34 dBi, high radiation efficiency of up to 89% and cross-polarization level below -20 dB are obtained. These characteristics all imply that the proposed antenna can be applied to WLAN and Car-to-Car (C2C) communications.


**INDEX TERMS** Multimode, patch antenna, shorting parasitic patch, metasurface, front-to-back ratio, radiation efficiency.

## I. INTRODUCTION

With the large-scale popularization of mobile Internet, IEEE proposed the 802.11p protocol in July 2010 as a supplementary protocol to 802.11 to meet the relevant applications of intelligent transportation systems (ITS) in dedicated short range communications (DSRC) system [1]. A direct communication through radio transmission between roadside, vehicle and portable radio equipment, enabling communication and exchange of information between vehicles, people and roadsides infrastructure. In the United States and Europe, Car-to-Car (C2C) and Car-to-Infrastructure (C2I), as two different application areas in DSRC [2] both work at 5.9 GHz (5.85-5.925 GHz). Successively, frequency bands

of 5.905-5.925 GHz is also released for intelligent networked car in China.

The wireless local area network (WLAN) working at 5.15-5.85 GHz supports IEEE 802.11a/n/ac protocol with a single-channel working bandwidth of up to 160 MHz and a transmission rate of up to 1 Gbps. Combining C2C communication that can obtain real-time information of the surrounding vehicles with the vehicle-mounted WLAN application that can access the Internet at any time can not only improve driving safety, but also provide users with more convenient services. Although, these advantages enhance the competitiveness of smart cars, the design of vehicle antenna becomes more complicated. Especially when the antenna is installed inside the vehicle, the radiation performance is correspondingly weakened due to the shielding effect [3]. Therefore, it is challenging and practical to design a broadband vehicle antenna with high gain characteristics.

The associate editor coordinating the review of this manuscript and approving it for publication was Debabrata Karmokar .

The existing literature presents a series of vehicle antennas for C2C communication with low profile, broadband, multi-band, and high gain characteristics. In [3], a triangular-shaped patch antenna is designed by combing V-shaped slot and shorting pins. Three resonant modes of  $TM_{10}$ ,  $TM_{20}$  and  $TM_{11}$  generated by the proposed design jointly promote the antenna to acquire an impedance bandwidth of up to 32.2%. However, the maximum gain of the antenna is only 6.5 dBi. Also affected by the shielding effect [4] inside the vehicle, the working efficiency of the antenna is also reduced. A shark-fin antenna composed of two monopole antennas is proposed in [5]. The designed antenna with the characteristic of triple-band and high efficiency can be utilized for mobile, WLAN and C2C application. But, the forward radiation is usually blocked due to the curvature of the roof. To solve this problem, a cavity antenna placed above the windshield is investigated in [6]. The designed cavity antenna located at the front of the roof can improve the coverage of the central roof antenna to other vehicles and pedestrians. In [7], a novel multi-service antenna is designed for automotive communication. The fabricated Y-shaped monopole operating at 5.85 GHz provides resonance for C2C and C2I services, and the isolation within the entire service bandwidth is greater than 15 dB. But the gain at 5.85 GHz is less than 2.5 dBi, which is not conducive to the realization of communication by cars on congested roads.

As mentioned above, the antennas currently utilized in automotive communication either have low radiation gain or narrow resonance bandwidth. To address these two issues, the introduction of gain-enhancing metasurfaces based on multimode resonance can significantly improve antenna gain and impedance bandwidth, and this approach has not been researched in the existing literature. Multimode resonance is one of the common methods to expand the bandwidth, and a large number of related works are recorded in the existing literature. Such as,  $TM_{10}$ ,  $TM_{12}$  and  $TM_{22}$  modes are obtained simultaneously by exciting the grid-slotted radiation patch with grounded balun feeding structure in [8]. In [9]–[12], multi-layer frequency-selective surface (FSS), shorting pins and substrate integrated suspended line (SISL) with U-shaped slot are introduced to acquire multimode resonance, respectively. However, the multi-layer structure with more than four layers and the additional feeding network greatly increase the design complexity and radiation loss.

In terms of improving antenna gain, a large number of related works are published one after another. Among them, partially reflective surfaces (PRS), as a metasurface with enhanced gain properties, is widely employed in the field of high-gain antennas. In [13]–[29], Fabry-Pérot cavity (FPC) antennas with the feature of broadband, high gain and compact structure are designed successively by introducing PRS layer. Attribute to the gain enhancement characteristic of PRS, the gain of some antennas is as high as 13 dBi or more. Especially in [18]–[19] and [22]–[24], it can be seen that the gain of the antenna is comparable to that of the array antenna. However, it is worth noting that the stacking structure of

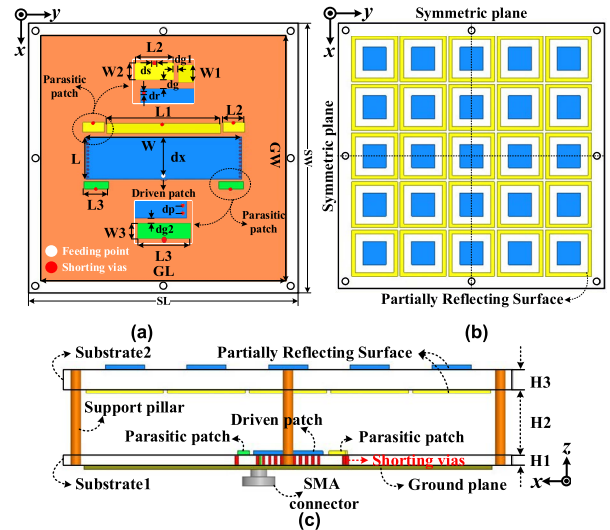


**FIGURE 1. Geometry of the proposed broadband patch antenna: (a) top view of the antenna; (b) top view of the PRS array; (c) side view of the assembled antenna.  $SL = 110$ ,  $SW = 110$ ,  $GL = 100$ ,  $GW = 100$ ,  $W = 63.5$ ,  $L1 = 46.5$ ,  $L2 = 8.75$ ,  $L3 = 10$ ,  $L = 17$ ,  $W1 = 4$ ,  $W2 = 4$ ,  $W3 = 3$ ,  $dg = 2$ ,  $dg1 = 1$ ,  $dg2 = 0.9$ ,  $dp = 1.5$ ,  $dr = 0.8$ ,  $ds = 1.0$ ,  $dx = 15.7$ ,  $H1 = 1.575$ ,  $H2 = 26$ ,  $H3 = 5$  (all dimensions in mm).**

the proposed antennas up to 5 layers not only increases the antenna loss and manufacturing cost, but also increases the design difficulty correspondingly.

In this paper, a multimode antenna with the features of broadband, high gain, high radiation efficiency, directional radiation and easy manufacturing is designed. A driven patch with both sides shorting fed directly by a coaxial probe is presented to generate the  $TM_{03}$  and  $TM_{11}$  modes. Five shorting parasitic patches are excited by coupling with the driven patch to obtain the  $TM_{21}$  mode. In order to improve the gain of the broadband patch antenna to the level of the array, a novel PRS is introduced. The presented PRS layer not only has little influence on the reflection coefficient, but also the reflection phase of PRS has a positive gradient characteristic. The measured results show that the assembled antenna has a radiation gain of up to 12.34 dBi which is capable for the errands of WLAN and C2C communication.

## II. ANTENNA DESIGN AND PRS ANALYSIS

The geometry of the designed antenna with the optimal parameters is given in Fig. 1. It can be seen that the proposed antenna is composed of two substrates. Among them, Rogers 5880 with relative permittivity of 2.2 is employed as substrate 1 which is located in the lower layer of the proposed antenna. A driven patch with both sides shorted is printed on the center of substrate 1 and a coaxial probe is utilized to excite the patch at a distance of 15.7 mm from the open end. Meanwhile, five shorting parasitic patches are printed on the two open ends of the driven patch to improve the impedance bandwidth. While, a ground plane is printed on the back of substrate 1. In order to improve antenna gain and the directivity of pattern, a PRS located on the top layer of the antenna is introduced. As depicted in Fig. 1(c), the filler of PRS layer

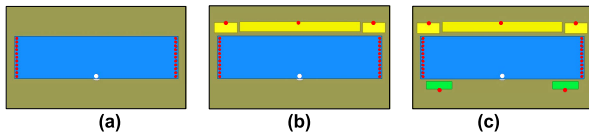


**FIGURE 2.** The evolution of the proposed broadband patch antenna. (a) Ant. 1; (b) Ant. 2; (c) Ant. 3.

is a F4BM substrate with a relative permittivity of 2.2. And  $5 \times 5$  periodically arranged square metal coatings and square rings are printed on the upper surface and the lower surface of the substrate 2 respectively. At last, eight support pillars made of polyamide are located between the two substrates for introducing an air layer with a height of 26 mm.

In order to clearly explain the characteristics of broadband and high gain for the designed antenna, the design theory of the broadband patch antenna and the analysis of the PRS layer will be further elaborated in Section A and Section B respectively.

### A. BROADBAND PATCH ANTENNA DESIGN

In Fig. 2, three antenna prototypes that evolve sequentially during the antenna design process are presented. Based on the cavity theory, the Ant. 1 is first proposed. A driven patch is printed on the center of the Rogers 5880 substrate, and shorting vias conforming to the following formula [30] are placed at the edges of the two short sides to introduce perfect electric walls.

$$dr < \lambda_0/5 \tag{1}$$

$$dp \leq 4dr \tag{2}$$

where  $dr$  represents the diameter of the periodic metal via,  $dp$  represents the distance between the centers of two adjacent metal vias and  $\lambda_0$  represents the cutoff wavelength. Since the thickness of the Rogers 5880 is smaller than the wavelength, two open ends of the driven patch can also be regarded as two perfect magnetic walls. Then, a cavity model is introduced to explain the resonance principle of Ant. 1. It can be obtained from [31]–[33] that when the cavity is working in  $TM_{mn}$  mode, the resonant frequency can be calculated by the following formula:

$$f_{TM_{mn}} = \frac{c}{2\pi\sqrt{\epsilon_r}} \sqrt{\left(\frac{m\pi}{L_e}\right)^2 + \left(\frac{n\pi}{W_e}\right)^2} \tag{3}$$

where  $\epsilon_r$  represents relative permittivity of the inner medium in the cavity,  $c$  represents the speed of light in free space.  $L_e$  and  $W_e$  represent the length and width of the cavity which can be calculated by equation (4) and (5), respectively.

$$W_e = W - \frac{(dr)^2}{0.95dp} \tag{4}$$

$$L_e = L + 2\Delta L \tag{5}$$

where  $\Delta L$  represents the extended part of the cavity length to compensate for the fringe field caused by the two opened ends of the cavity.

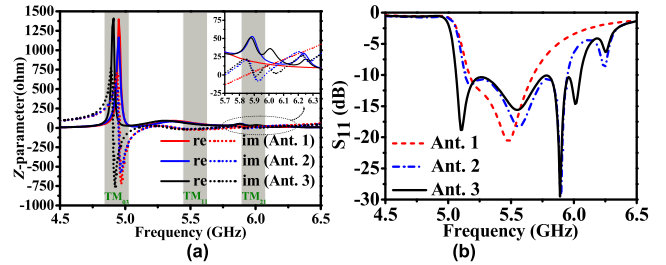


**FIGURE 3.** Comparison of the simulated results for the three antennas. (a) Input impedance; (b) S11.

It can be seen from Fig. 3(a) that  $TM_{03}$  and  $TM_{11}$  modes of Ant. 1 are obtained respectively at 4.95 GHz and 5.38 GHz. Due to the adjacent dual-mode resonance, the Ant. 1 with an impedance bandwidth of 9.6% exhibits broadband characteristic. In order to further expand the bandwidth on the basis of dual-mode resonance, three shorting parasitic patches are placed on the open end of the cavity. Then, Ant. 2 is proposed and the  $TM_{21}$  mode is also introduced on the parasitic patches through coupling effect. Comparing the input impedance of Ant. 1 and Ant. 2 in Fig. 3(a), it can be found that the input impedance of Ant. 2 at 5.9 GHz is  $Z_{in} = 49.72 - j2.37$ , which satisfies the impedance matching condition. The better impedance characteristic of Ant. 2 is also consistent with the excellent reflection coefficient of Ant. 2 at 5.9 GHz in Fig. 3(b). Combining the  $TM_{03}$ ,  $TM_{11}$  and  $TM_{21}$  modes generated by the Ant. 2, an impedance bandwidth of 14.6% from 5.14 GHz to 5.95 GHz is acquired. Based on the Ant. 2, Ant. 3 is designed by loading two additional shorting parasitic patches on the other open end of the cavity to optimize the input impedance at 6.0 GHz. It can also be seen from Fig. 3 that the Ant. 3 has an impedance bandwidth of 17.6% from 5.07 GHz to 6.05 GHz. Fig. 4 shows the electric field distribution of Ant. 3 at 5.5 GHz, 5.9 GHz and 6.0 GHz. It can be concluded that the resonance at 5.5 GHz is mainly dominated by the driven patch, while the resonance at 5.9 GHz is generated by three shorting parasitic patches on the same side of the open end. In contrast, the two additional shorting parasitic patches close to the other open end of the cavity have a greater impact on the resonance at 6.0 GHz.

### B. ANALYSIS OF PRS UNIT CELL

In [16], G. V. Trentini first proposed placing a partially reflective surface above the antenna. Then, the antenna ground plane and the partially reflective surface constitute a resonant cavity, in which electromagnetic waves are repeatedly reflected to increase the antenna radiation gain. Moreover, the resonant frequency of the cavity and the height of the cavity satisfy the following formula [23]–[24], [26]:

$$f = \frac{c}{4\pi h} (\varphi_p + \varphi_g - 2N\pi), \quad N = 0, 1, 2, 3, \dots \tag{6}$$

where,  $h$  represents the distance between the PRS and the ground plane,  $\varphi_p$  and  $\varphi_g$  represent the reflection phase of the PRS and the ground plane, and  $f$  represents the resonance frequency of the resonant cavity. In order to reduce the height

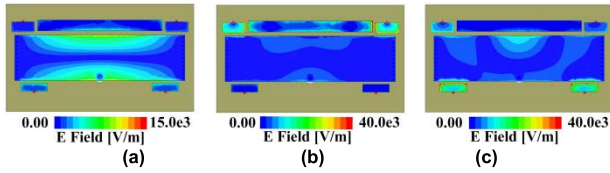


FIGURE 4. Simulated electric field distribution of the proposed Ant. 3. (a) 5.5 GHz; (b) 5.9 GHz; (c) 6.0 GHz.

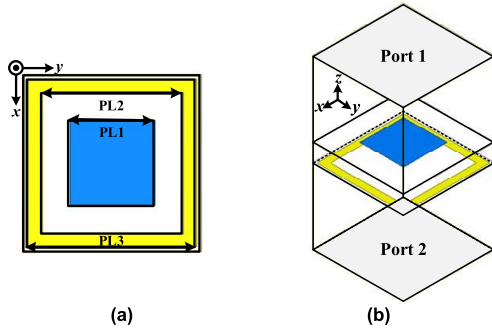


FIGURE 5. (a) Schematic of the proposed PRS unit cell. PL1 = 9.6, PL2 = 16, PL3 = 19 (all dimensions in mm); (b) simulation setup of the proposed PRS unit cell.

of the resonant cavity in practical applications,  $N$  usually takes a value of 0. Not only that, the corresponding reflection phase of the ground plane composed of a total reflection perfect electrical conductor (PEC) is also taken as  $\pi$ . Therefore, equation (6) can be converted to equation (7).

$$\varphi_p = \frac{f4\pi h}{c} - \pi \quad (7)$$

It can be obtained from equation (7) that when the cavity height  $h$  is determined and the reflection phase of the PRS  $\varphi_p$  increases with the increase of frequency, the characteristics of high-gain radiation can be achieved in a large bandwidth. In other words, the PRS reflection phase within the working bandwidth has a positive gradient. Assuming that the reflection amplitude  $\rho$  of the partially reflective surface is constant or approximately constant in a certain frequency band, the 3-dB gain bandwidth of this antenna model can be calculated by equation (8) [34].

$$BW_{3dB} = \frac{1 - \rho}{\sqrt{\rho}} \frac{\lambda}{2h\pi} \quad (8)$$

Among them,  $\lambda$  is the wavelength of the center frequency in free space. Combining equation (7) and equation (8), it can be obtained that a PRS with positive gradient reflection phase and stable reflection amplitude within the operation bandwidth is essential for high gain and broadband characteristics. In view of this feature, a novel PRS with wideband and positive gradient is investigated in this section to improve radiation gain of the broadband patch antenna. The configuration and simulation model of the PRS unit are shown in Fig. 5. A F4BM substrate with a thickness of 5 mm and relative permittivity of 2.2 is selected as the filler for the PRS unit. A square patch and a square ring with the optimal dimension are printed on the upper and lower surfaces of the F4BM to

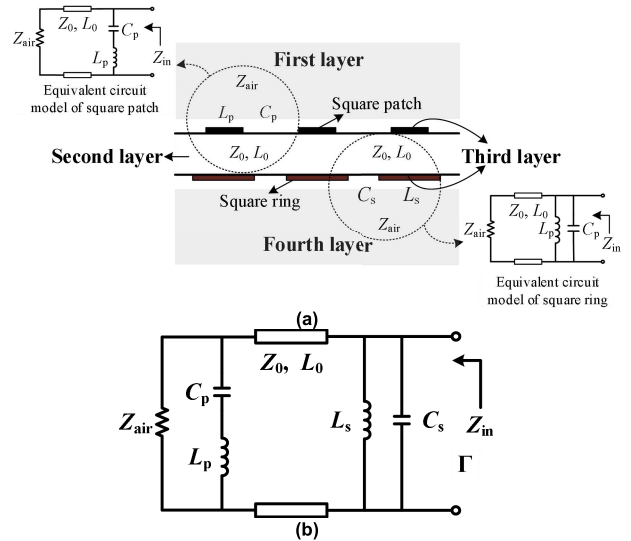
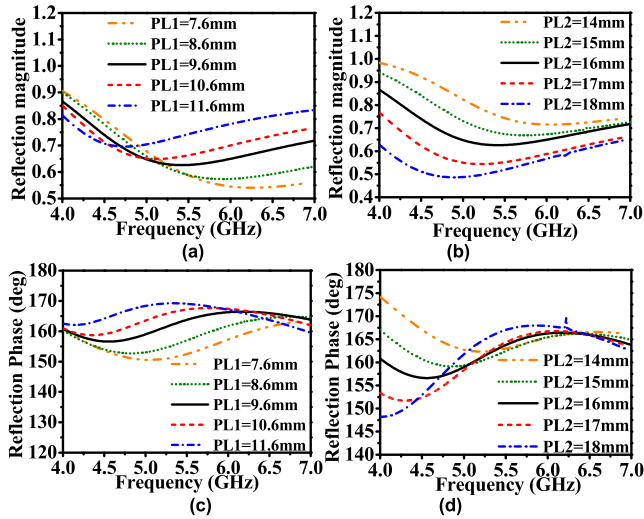


FIGURE 6. (a) PRS hierarchical structure diagram and (b) the equivalent lumped circuit diagram of the PRS unit.

support the in-phase feature between the reflected wave from the ground plane and the reflection phase of the PRS.

In order to explain the working principle of the PRS vividly, we subdivide the PRS into four layers, as shown in Fig. 6(a). The uppermost layer is a free space that can extend infinitely at one end. In the lumped circuit model, the free space can be seen as a broadband load  $Z_{air}$  which is equivalent to the wave impedance of a plane wave. The second layer is the F4BM substrate, which can be equivalent to a microstrip transmission line with a characteristic impedance of  $Z_0$  and an electrical length of  $L_0$ . The metal patch printed on the surface of the F4BM is classified as the third layer. Due to the inductance of the square patch  $L_p$  and the capacitance  $C_p$  caused by the gap between the adjacent square patches, a series LC circuit is realized. On the contrary, the inductance of the square ring  $L_s$  and the capacitance  $C_s$  introduced by the adjacent square rings form a parallel LC circuit. Then, the two LC oscillating circuits form a parallel circuit as shown in Fig. 6(b) through a transmission line equivalent to the F4BM substrate. The last layer is the semi-infinite free space below the PRS, which is also the direction where the electromagnetic wave incident source of the entire circuit is located. Since it is the same as the semi-infinite free space above the PRS, it can also be equivalent to a broadband load with a characteristic impedance of  $Z_{air}$ . When electromagnetic waves are incident perpendicularly from below the PRS, the electromagnetic waves are reflected between the third layer and the fourth layer. Attribute to the partial reflection effect of the PRS, the transmitted waves are superimposed in phase on the first layer, which improves the radiation gain. As shown in Fig. 6(b), the equivalent lumped circuit diagram of the PRS unit is presented, and  $Z_{in}$  represents the input impedance,  $\Gamma$  represents the reflection coefficient of the lumped circuit, which is equivalent to the reflection characteristic of the proposed PRS.



**FIGURE 7.** The simulated results of the PRS unit. (a) Reflection amplitude changing with PL1, (b) reflection amplitude changing with PL2, (c) reflection phase changing with PL1, and (d) reflection phase changing with PL2.

On the one hand, the F4BM substrate acts as a filler between the square patch and the square ring, which changes the inductance  $L$  and capacitance  $C$  in the lumped circuit model. Moreover, the substrate with thickness of  $H_3$  and relative permittivity of  $\epsilon_r$  is equivalent to a transmission line, which can produce impedance transformation effects on the subsequent cascaded circuits. On the other hand, since the square patch is located at the center of the aperture formed by the square ring, the capacitance of the square ring is greatly increased [13]. Finally, a band-pass PRS structure is obtained. In order to further verify the working mechanism of the PRS unit, a parameter analysis is carried out on the length of the square patch PL1 and the short side of the square ring PL2. The corresponding simulated results are shown in Fig. 7 and it can be concluded from Fig. 7(a) that the reflection amplitude of the PRS unit increases with the increase of PL1, especially in the high frequency range of 5.0-7.0 GHz. However, compared with PL1, the effect of PL2 on the reflection amplitude is completely opposite as shown in Fig. 7(b). The reason for this phenomenon is that as the size of the square patch increases, its equivalent inductance in the lumped circuit also increases. On the contrary, as PL2 increases, the aperture formed by the square ring also increases, resulting in a larger capacitance between the upper and lower patches. In Fig. 7, the simulated reflection phase is also given. It can be obtained that with the change of PL1, the reflection phase at 5.5 GHz fluctuates from  $150^\circ$  to  $170^\circ$ , and the reflection phase still maintains a positive gradient in the range of 5.0-6.0 GHz. While, the effect of PL2 on the reflection phase is mainly concentrated in 4.0-5.0 GHz. Considering the stability of the reflection amplitude and the positive gradient of the reflection phase in the working bandwidth, the optimal values of PL1 and PL2 are set to 9.6 mm and 16 mm, respectively.

Based on the above theory and simulation analysis, a  $5 \times 5$  array is designed to improve the broadband antenna gain.

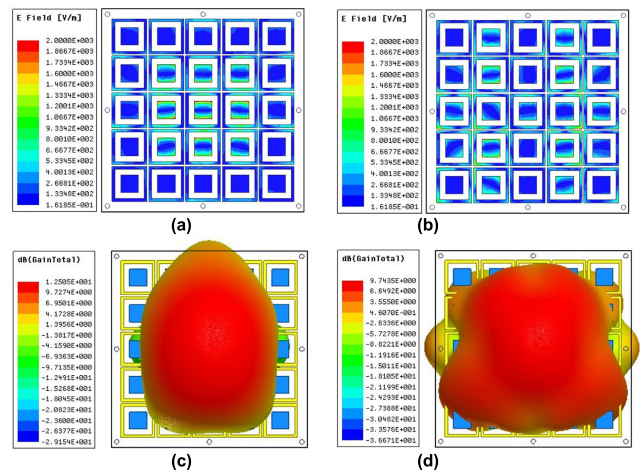


**FIGURE 8.** Simulated electric field distribution of the proposed  $5 \times 5$  PRS and the simulated 3-D radiation pattern of the assembled antenna. (a) Electric field distribution at 5.5 GHz, (b) electric field distribution at 6.0 GHz, (c) simulated 3-D radiation pattern at 5.5 GHz, and (d) simulated 3-D radiation pattern at 6.0 GHz.

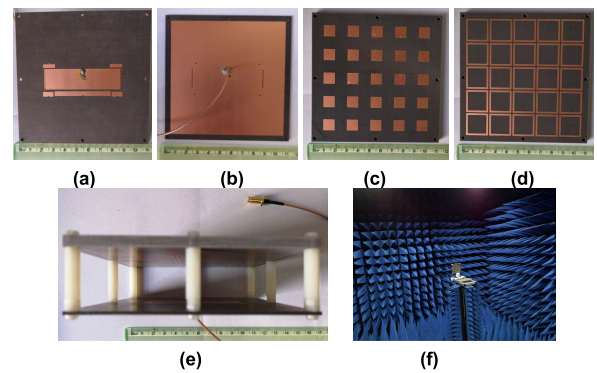


**FIGURE 9.** Photographs and test procedures of the antenna prototype. (a) The upper surface of the fabricated broadband patch antenna, (b) the lower surface of the fabricated broadband patch antenna, (c) the upper surface of the fabricated  $5 \times 5$  PRS array, (d) the lower surface of the fabricated  $5 \times 5$  PRS array, (e) side view of the assembled antenna, and (f) antenna test scenario.

According to equation (6) and further simulation, the distance  $H_3$  between the PRS layer and the radiating antenna is set to 26 mm. Moreover, the length and width of the PRS array are both 110 mm, which ensures that the assembled antenna can be installed on the roof or above the license plate. Fig. 8 shows the electric field distribution of the PRS array at 5.5 GHz and 6.0 GHz. It can be seen from Fig. 8 that the electric field density at the center of the array is significantly higher than the edge of the array at 5.5 GHz. While the electric field at 6.0 GHz is widely distributed in the four directions of the array. The different electric field distributions at the two frequency points are consistent with the 3-D radiation patterns of the assembled antenna shown in Fig. 8(c) and Fig. 8(d).

### III. MEASURED RESULTS DISCUSSION

As shown in Fig. 9, the proposed broadband patch antenna and  $5 \times 5$  PRS array are fabricated to verify the accuracy of the above theoretical analysis. Meanwhile, eight nylon pillars

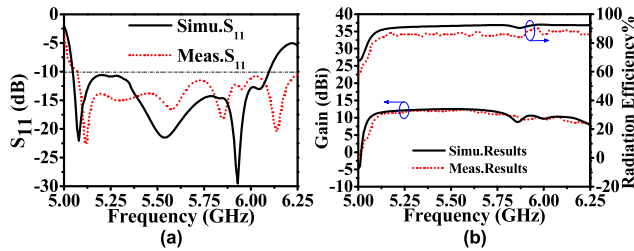


**FIGURE 10.** Simulated and measured results of the fabricated high gain broadband patch antenna. (a)  $S_{11}$  and (b) gain and radiation efficiency.

in Fig. 9(e) are employed to fix the patch antenna and the PRS array. A test process shown in Fig. 9(f) is also implemented on the assembled antenna to measure the antenna gain, radiation pattern and radiation efficiency.

The measured result and simulated result of  $S_{11}$  are given in Fig. 10(a). It can be found that the measured bandwidth from 5.08 GHz to 6.25 GHz is basically consistent with the simulated result, except for a slight shift to high frequency. Meanwhile, in Fig. 10(b) the measured gain of up to 12.34 dBi in 5.15-5.85 GHz can be utilized for WLAN. And a gain of up to 9.47 dBi which can be used for C2C communication in 5.905-5.925 GHz is also obtained. In a nutshell, the features of high gain in this paper is more attractive than the antennas in [2]–[5], [7] and [18]. However, the measured maximum gain of 12.34 dBi is slightly less than the simulated gain of 12.50 dBi due to the deviation in the welding and testing process. In Fig. 10(b), the measured results show that up to 89% radiation efficiency is obtained within the 20.7% operating bandwidth. Fig. 11 shows the measured results and simulated results of the radiation patterns at 5.1 GHz, 5.5 GHz and 5.9 GHz. It can be seen that the measured co-polarization shows excellent directivity with a front-to-back ratio better than 15 dB and the measured results of the cross-polarization level in the main beam direction are all lower than  $-20$  dB. In addition, when the designed antenna operates at 5.9 GHz, the attractive 3-dB beamwidth of E-plane and H-plane up to  $102^\circ$  and  $94^\circ$ , respectively, increases the communication coverage of C2C and C2I. Especially when the antenna is installed near the license plate, the communication scenario is shown in Fig. 12.

#### IV. COMPARISON

In order to highlight the advantages for this design, Table 1 presents the comparison results of the investigated patch antenna with the reported antennas in terms of impedance bandwidth, 3-dB gain BW, radiation efficiency, maximal gain, size and radiation pattern.

In [1], four L-shaped antennas and two feeding networks are integrated to design a dual-port antenna array for vehicular environment. However, the measured results show that the impedance bandwidth and radiation efficiency of the antenna are only 1.27% and 65%. In [4], a monopolar patch antenna with the advantages of wideband and high radiation efficiency is proposed. But the low gain and high cross-polarization are not conducive to the application of the antenna in complex

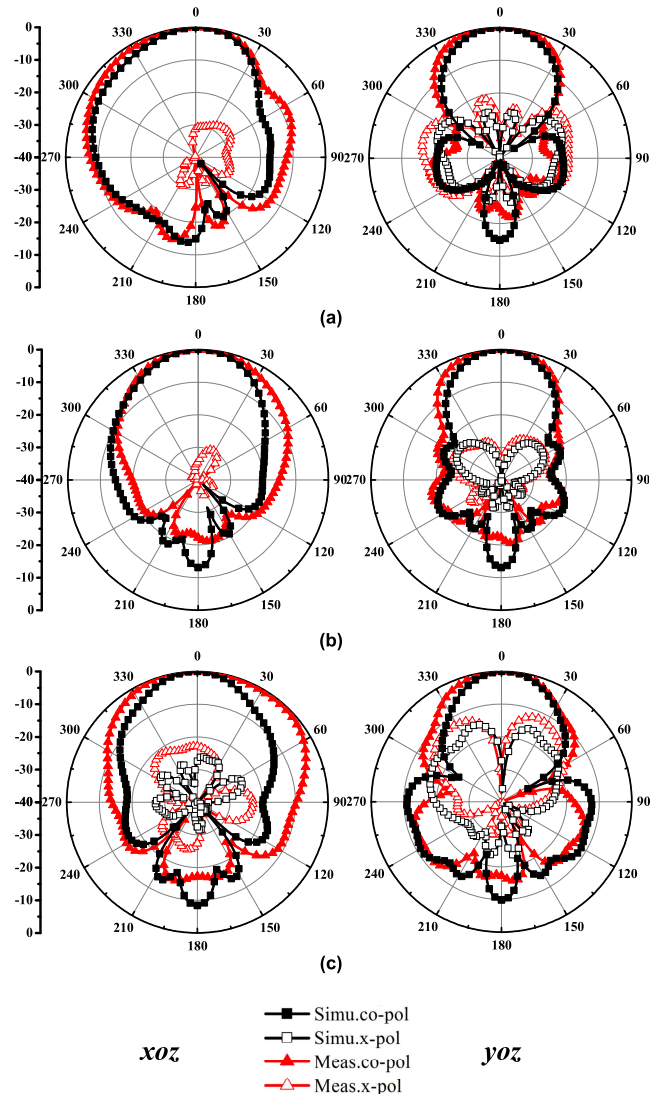


**FIGURE 11.** Simulated and measured radiation patterns of the proposed antenna in xoz and yoz planes. (a) 5.1GHz, (b) 5.5 GHz, and (c) 5.9 GHz.

electromagnetic environments. A multi-service antenna is investigated in [7] for automotive communications. Although the measured results show that the antenna can be applied in DCS1800, IEEE 802.11b/g/n, C2C and C2I fields, the measured maximum efficiency and gain of the antenna are only 70% and 3 dBi in 5.8-5.9 GHz.

Compared with the multimode antenna in [8]–[12], three resonant modes can be obtained using only a simple coaxial probe and shorting patch without introducing additional losses and backlobe radiation. In [18], a patch antenna for vehicle blind spot area communication is designed, but the problems of narrowband and low gain are still not solved. In [20]–[29], metasurfaces are introduced to design high-gain antennas. Although the impedance bandwidth better than 20% and the gain higher than 14 dBi are achieved in the latest papers [22]–[24] and [26]–[28], the complex multi-layer structure increases the difficulty of antenna design and manufacture. The double-layer structure adopted by the high-gain

TABLE 1. Comparison between reported antenna and the proposed multimode broadband high-gain antenna.

Ref	IMBW (%)	3-dB gain BW (%)	$f_{min}$ (GHz)	Effi (%)	MG (dBi)	Size ( $\lambda_{min}^2$ )	Height ( $\lambda_{min}$ )	RT	Num. of layer	Application field Feed Type
[1]	1.27	1.27	5.85	65	7.0	$1.56 \times 1.17$	0.13	End fire	1	C2C
[4]	32.20	-	4.82	93	6.5	$1.03 \times 1.03$	0.05	Omnidirectional	1	C2C & WLAN
[7]	10 & 11.4 7.5 & 7.6	-	1.8	90	3.0	$0.61 \times 0.45$	0.005	Omnidirectional	1	2G & 4G & WiMAX & C2C
[18]	11.16	-	3.49	-	5.2	$0.35 \times 0.35$	0.21	Directional	2	C2C
[20]	14.1	-	8.25	25.6	11.2	$1.81 \times 1.81$	0.3	Directional	2	Low-RCS platform
[21]	15.5	14.8	13.1	-	13.8	$2.61 \times 2.61$	0.61	Directional	2	-
[22]	91.1	86.3	5.8	-	14.2	$1.0 \times 1.0$	0.71	Directional	5	-
[23]	25.1	25.1	8.88	-	13.92	$1.95 \times 1.95$	0.55	Directional	3	-
[24]	21.4	-	25	-	15.4	$5.0 \times 4.0$	0.54	Unidirectional	2	5G
[25]	1.5 & 2.2	-	3.42	77	16.8	$1.6 \times 1.6$	0.56	Directional	3	-
[26]	32.7	34.2	9.2	-	14.2	$4.1 \times 4.1$	0.5	Directional	4	Navigation & Positioning
[27]	37.2	32.3	10.5	-	14	$4.65 \times 4.65$	0.53	Directional	3	-
[28]	22.8	-	13.48	89.2	21.59	$2.69 \times 4.35$	0.54	Directional	3	MIMO
[29]	5.03	1.5	11.61	-	16.22	$3.88 \times 3.88$	0.22	Directional	3	X-band
<b>This work</b>	<b>20.7</b>	<b>18.1</b>	<b>5.08</b>	<b>89</b>	<b>12.3</b>	<b><math>1.86 \times 1.86</math></b>	<b>0.55</b>	<b>Directional</b>	<b>2</b>	<b>C2C &amp; WLAN</b>

$f_{min}$  represents minimum frequency point within the resonance bandwidth; MG represents maximal gain;  $\lambda_{min}$  represents wavelength of  $f_{min}$  in free space; RT represents radiation type.

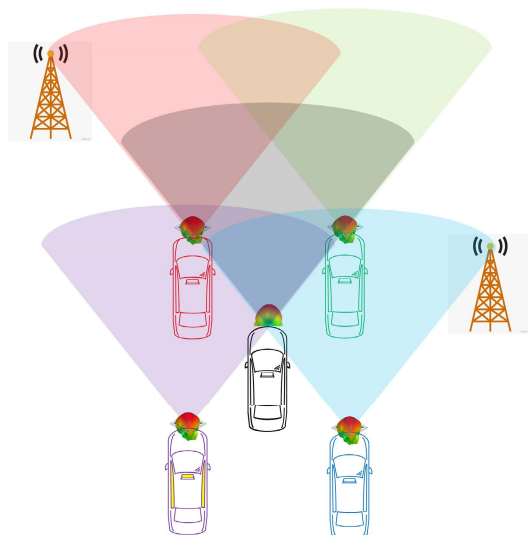


FIGURE 12. Simulation diagram of vehicle-to-vehicle communication and vehicle-to-base station communication.

multimode antenna designed in this paper is beneficial to the high-efficiency radiation. Furthermore, the resonant frequency lower than 6 GHz, the size of  $1.86 \lambda_{min} \times 1.86 \lambda_{min}$  and the directional radiation with a FBR better than 15 dB all imply that the antenna is a suitable candidate for C2C and WLAN communication.

### V. CONCLUSION

A multimode antenna with the features of broadband, high gain, high efficiency radiation and excellent FBR is investigated in this paper. Shorting parasitic patch and the metasurfaces technology are combined to obtain additional  $TM_{21}$  mode and a gain boost effect within the whole resonance bandwidth. The impedance bandwidth of up to 20.7% the radiation gain of up to 12.3 dBi and the directional radiation pattern all show that the antenna can be employed for WLAN and C2C communication. Furthermore, when the proposed antenna works in C2C communication, the measured antenna gain is higher than [1], [3], [7], [18], [20], which indicates that the design is more suitable for application in scenarios [4]. Compared with the multimode antennas [8]–[12] and high-gain FPC antennas [19]–[29] in the existing papers, the simple shorting patch and novel PRS structure can improve the narrowband and low gain without introducing additional feeding structure or increasing the difficulty of antenna design.

### REFERENCES

- [1] F. Liu, Z. J. Zhang, W. H. Chen, Z. H. Feng, and M. F. Iskander, "An endfire beam-switchable antenna array used in vehicular environment," *IEEE Antennas Wireless Propag. Lett.*, vol. 9, pp. 195–198, 2010.
- [2] M. Boban and P. M. D'Orey, "Exploring the practical limits of cooperative awareness in vehicular communications," *IEEE Trans. Veh. Technol.*, vol. 65, no. 6, pp. 3904–3916, Jun. 2016.

- [3] T. Abbas, J. Karedal, and F. Tufvesson, "Measurement-based analysis: The effect of complementary antennas and diversity on vehicle-to-vehicle communication," *IEEE Antennas Wireless Propag. Lett.*, vol. 12, pp. 309–312, 2013.
- [4] H. Wong, K. K. So, and X. Gao, "Bandwidth enhancement of a monopolar patch antenna with V-shaped slot for car-to-car and WLAN communications," *IEEE Trans. Veh. Technol.*, vol. 65, no. 3, pp. 1130–1136, Mar. 2016.
- [5] D. V. Navarro-Méndez, L. F. Carrera-Suárez, D. Sánchez-Escuderos, M. Cabedo-Fabrés, M. Baquero-Escudero, M. Gallo, and D. Zamberlan, "Wideband double monopole for mobile, WLAN, and C2C services in vehicular applications," *IEEE Antennas Wireless Propag. Lett.*, vol. 16, pp. 16–19, 2017.
- [6] G. Artner, W. Kotterman, G. D. Galdo, and M. A. Hein, "Conformal automotive roof-top antenna cavity with increased coverage to vulnerable road users," *IEEE Antennas Wireless Propag. Lett.*, vol. 17, no. 12, pp. 2399–2403, Dec. 2018.
- [7] M. G. N. Alsath and M. Kanagasabai, "A shared-aperture multiserive antenna for automotive communications," *IEEE Antennas Wireless Propag. Lett.*, vol. 13, pp. 1417–1420, 2014.
- [8] B. Cheng, Z. Du, and D. Huang, "A broadband low-profile multimode microstrip antenna," *IEEE Antennas Wireless Propag. Lett.*, vol. 18, no. 7, pp. 1332–1336, Jul. 2019.
- [9] X. Zhong, H.-X. Xu, L. Chen, W. Li, H. Wang, and X. Shi, "An FSS-backed broadband phase-shifting surface array with multimode operation," *IEEE Trans. Antennas Propag.*, vol. 67, no. 9, pp. 5974–5981, Sep. 2019.
- [10] W. Hu, C. Li, X. Liu, L. Wen, T. Feng, W. Jiang, and S. Gao, "Wideband circularly polarized microstrip patch antenna with multimode resonance," *IEEE Antennas Wireless Propag. Lett.*, vol. 20, no. 4, pp. 533–537, Apr. 2021.
- [11] D.-F. Guan, Z.-P. Qian, W.-Q. Cao, L.-Y. Ji, and Y.-S. Zhang, "Compact SIW annular ring slot antenna with multiband multimode characteristics," *IEEE Trans. Antennas Propag.*, vol. 63, no. 12, pp. 5918–5922, Dec. 2015.
- [12] J. Hao, N. Yan, Y. Luo, H. Fu, and K. Ma, "A low-cost dual-band multimode high-gain stacked-patch antenna based on SISL for 5G applications," *IEEE Antennas Wireless Propag. Lett.*, vol. 21, no. 1, pp. 4–8, Jan. 2022.
- [13] A. Hosseini, F. De Flaviis, and F. Capolino, "Design formulas for planar Fabry–Pérot cavity antennas formed by thick partially reflective surfaces," *IEEE Trans. Antennas Propag.*, vol. 64, no. 12, pp. 5487–5491, Dec. 2016.
- [14] Y.-H. Lv, X. Ding, and B.-Z. Wang, "Dual-wideband high-gain Fabry–Pérot cavity antenna," *IEEE Access*, vol. 8, pp. 4754–4760, 2020.
- [15] T. Li and Z. N. Chen, "Shared-surface dual-band antenna for 5G applications," *IEEE Trans. Antennas Propag.*, vol. 68, no. 2, pp. 1128–1133, Feb. 2020.
- [16] G. Von Trentini, "Partially reflecting sheet arrays," *IRE Trans. Antennas Propag.*, vol. 4, no. 4, pp. 666–671, Oct. 1956.
- [17] B. A. Munk, *Finite Antenna Array and FSS*. Hoboken, NJ, USA: Wiley, 2003.
- [18] T. Mondal, S. Maity, R. Ghatak, and S. R. B. Chaudhuri, "Compact circularly polarized wide-beamwidth Fern-fractal-shaped microstrip antenna for vehicular communication," *IEEE Trans. Veh. Technol.*, vol. 67, no. 6, pp. 5126–5134, Jun. 2018.
- [19] R. M. Hashmi and K. P. Esselle, "Enhancing the performance of EBG resonator antennas by individually truncating the superstructure layers," *IET Microw., Antennas Propag.*, vol. 10, no. 10, pp. 1048–1055, Jul. 2016.
- [20] K. Li, Y. Liu, Y. Jia, and Y. J. Guo, "A circularly polarized high-gain antenna with low RCS over a wideband using chessboard polarization conversion metasurfaces," *IEEE Trans. Antennas Propag.*, vol. 65, no. 8, pp. 4288–4292, Aug. 2017.
- [21] M. A. Meriche, H. Attia, A. Messai, S. S. I. Mitu, and T. A. Denidni, "Directive wideband cavity antenna with single-layer meta-superstrate," *IEEE Antennas Wireless Propag. Lett.*, vol. 18, no. 9, pp. 1771–1774, Sep. 2019.
- [22] N. Nguyen-Trong, H. H. Tran, T. K. Nguyen, and A. M. Abbosh, "Wideband Fabry–Pérot antennas employing multilayer of closely spaced thin dielectric slabs," *IEEE Antennas Wireless Propag. Lett.*, vol. 17, no. 7, pp. 1354–1358, Jul. 2018.
- [23] F. Meng and S. K. Sharma, "A wideband resonant cavity antenna with compact partially reflective surface," *IEEE Trans. Antennas Propag.*, vol. 68, no. 2, pp. 1155–1160, Feb. 2020.
- [24] A. Goudarzi, M. M. Honari, and R. Mirzavand, "A high-gain leaky-wave antenna using resonant cavity structure with unidirectional frequency scanning capability for 5G applications," *IEEE Access*, vol. 9, pp. 138858–138865, 2021.
- [25] Z.-G. Liu, R.-J. Yin, Z.-N. Ying, W.-B. Lu, and K.-C. Tseng, "Dual-band and shared-aperture Fabry–Pérot cavity antenna," *IEEE Antennas Wireless Propag. Lett.*, vol. 20, no. 9, pp. 1686–1690, Sep. 2021.
- [26] Y. Guan, Y.-C. Jiao, Y.-D. Yan, Y. Feng, Z. Weng, and J. Tian, "Wideband and compact Fabry–Pérot resonator antenna using partially reflective surfaces with regular hexagonal unit," *IEEE Antennas Wireless Propag. Lett.*, vol. 20, no. 6, pp. 1048–1052, Jun. 2021.
- [27] M. W. Niaz, Y. Yin, R. A. Bhatti, Y.-M. Cai, and J. Chen, "Wideband Fabry–Pérot resonator antenna employing multilayer partially reflective surface," *IEEE Trans. Antennas Propag.*, vol. 69, no. 4, pp. 2404–2409, Apr. 2021.
- [28] W. Wang and Y. Zheng, "Wideband gain enhancement of high-isolation Fabry–Pérot antenna array with tandem circular parasitic patches and radial gradient PRS," *IEEE Trans. Antennas Propag.*, vol. 69, no. 11, pp. 7959–7964, Nov. 2021.
- [29] M. Y. Jamal, M. Li, K. Lawrence Yeung, X. Li, L. Jiang, and T. Itoh, "A low-profile Fabry–Pérot cavity antenna using anisotropic metasurface," *IEEE Antennas Wireless Propag. Lett.*, vol. 21, no. 2, pp. 356–360, Feb. 2022.
- [30] M. Mujumdar and A. Alphones, "Eighth-mode substrate integrated resonator antenna at 2.4 GHz," *IEEE Antennas Wireless Propag. Lett.*, vol. 15, pp. 853–856, 2016.
- [31] C. Balanis, *Antenna Theory: Analysis and Design*. Hoboken, NJ, USA: Wiley, 2005.
- [32] H. Kang and S. Lim, "Electrically small dual-band reconfigurable complementary split-ring resonator (CSRR)-loaded eighth-mode substrate integrated waveguide (EMSIW) antenna," *IEEE Trans. Antennas Propag.*, vol. 62, no. 5, pp. 2368–2373, May 2014.
- [33] Y. Seo, M. U. Memon, and S. Lim, "Microfluidic eighth-mode substrate-integrated-waveguide antenna for compact ethanol chemical sensor application," *IEEE Trans. Antennas Propag.*, vol. 64, no. 7, pp. 3218–3222, Jul. 2016.
- [34] A. P. Feresidis and J. C. Vardaxoglou, "High gain planar antenna using optimized partially reflective surfaces," *Proc. Inst. Elect. Eng. Microw. Antennas Propag.*, vol. 148, no. 6, pp. 345–350, Dec. 2001.



**YQIANG ZHENG** received the B.S. and M.S. degrees in physics and electronics communication engineering from Anhui Normal University, in 2004 and 2009, respectively. He is currently pursuing the Ph.D. degree with the China University of Mining and Technology.

He is currently a Professor with the School of Intelligent Manufacturing, Huainan Union University. His research interests include microstrip antennas, metamaterial, MIMO antennas, and 5G communications.



**MIN GAO** received the B.S. and M.S. degrees in electronic information engineering from the Anhui University of Science and Technology, in 2003 and 2013, respectively. She is currently pursuing the Ph.D. degree with the China University of Mining and Technology.

She is currently a Professor with the School of Mechanical and Electrical Engineering, Hefei Technology College. Her main research interests include intelligent signal processing, 5G communications, and vehicle-mounted networks.



**XIAOHU ZHAO** received the B.S. degree in industrial automation and the M.S. and Ph.D. degrees from the China University of Mining and Technology, Xuzhou, China, in 1998 and 2007, respectively.

He is currently an Associate Professor with the School of Information and Telecommunications, China University of Mining and Technology. His main research interests include the mine Internet of Things, mine communications, monitoring and control, computer networks, and intelligent computing.

...